Research article

Journal of RAMAN SPECTROSCOPY

Received: 4 May 2012 Revised: 31 August 2012 Accepted: 3 September 2012 Published online in Wiley Online Library: 16 October 2012

(wileyonlinelibrary.com) DOI 10.1002/jrs.4191

The use of Raman spectroscopy to characterize the carbon materials found in Amazonian anthrosoils

J. Ribeiro-Soares,[a] L. G. Cançado,[a] N. P. S. Falcão,[b] E. H. Martins Ferreira,[c] C. A. Achete[c] and A. Jorio[a]*

This manuscript presents the Raman characterization of the stable carbon materials found in a special type of soil, named *Terra Preta de Índio* (Indian Dark Earths). The *Terras Pretas de Índios* have been studied as a potential model for sustainable agriculture in the humid tropics. The stability of organic matter and the long-term high-level of ion exchange capacity in these soils are due to unusually high amount of black carbon. Here, we show how Raman spectroscopy can be used to characterize the stable carbon content in the *Terras Pretas de Índios* (TPI-carbons). The tangential stretching mode (G band) and the disorder-induced mode (D band) are analyzed in comparison to laboratory-produced amorphous carbons at different degree of disorder used here as reference materials. Statistical analysis show predominance of sp^2 phase and crystallite sizes within the limit range between nanographite and amorphous carbons, while Raman mapping of a TPI-carbon grain shows that the surface is more disordered than the grain core. The analysis used here can also differentiate the TPI-carbon structures from different types of charcoal. Copyright © 2012 John Wiley & Sons, Ltd.

Supporting Information may be found in the online version of this article.

Keywords: soil science; Terra Preta de Índio; carbon

Introduction

This work is focused on the Raman characterization of the stable carbon materials found in a special type of soil, named *Terra Preta de Índio*. Our goal is to show how Raman spectroscopy combined with previous knowledge in the field of carbon nanostructures can be applied in this soil science problem, which might have implications in greenhouse and anthropology studies.

What are Terras Pretas de Índios and why to study them

Terras Pretas de Índios (TPIs or Indian Dark Earths) are extremely fertile soils found in Northern Brazil,[1] in patches with average size of 20 ha.[2] The origin of this material may be anthropogenic from Pre-Columbian civilizations,[3] in an accumulation and burning process of organic matter intentionally or as a by-product of the occupation of these areas. Unlike the soils found in adjacent regions marked by low nutrient retention due to heavy rains, high temperatures, and humidity that eventually accelerate the organic matter degradation, the TPIs show high stability and recalcitrance,[4–6] keeping them fertile even after several years.

Previous studies performed by ^{13}C Nuclear Magnetic Resonance comparing the soil organic matter of TPIs with that found in adjacent soils have shown higher amounts of aromatic structures, and the process of burning (charring) of organic matter is responsible for the formation of such structures.[7,8] The large amount of black carbon (up to 70 times more than in adjacent soils)[9] has been related to the stability of soil organic matter. Such stability is essential to maintain the long-term productivity and to improve the cation exchange capacity,[5] which is essential to increase nutrient retention in highly leached soils of tropical regions.

The artificial reproduction of Amazonian anthropogenic TPI soils has been subject of many studies to improve soil quality.[4,10–13] Furthermore, the model of slash and burn is the outlook for the stock of carbon from the atmosphere through the burning of organic matter under controlled conditions, which may help to reduce the human activity effects on the environment due to the greenhouse effect.[12–14] Unfortunately the knowledge of how the TPI soils were produced is lost.[2,15]

Structural information about the carbon materials found in the TPIs (from now on called TPI-carbons) helps to reveal the origin of this material and to explain its superiority in terms of fertility (TPIs have twofold higher cation exchange capacity than adjacent soils with the same amount of carbon.[5]) Recent studies[16] have shown that the dominant structure of the TPI-carbons is convenient to promote a balance that ensures, at the same time, the reactivity of the soil (necessary to an optimal flow of nutrients between the soil and plants) and differentiated stability that sustains the quality of these sites for periods of millennia.[13,15–17]

* *Correspondence to: A. Jorio, Departamento de Física, ICEx, Universidade Federal de Minas Gerais, Belo Horizonte, MG, 30123-970, Brazil. E-mail: adojorio@fisica.ufmg.br*

a *Departamento de Física, ICEx, Universidade Federal de Minas Gerais, Belo Horizonte, MG, 30123-970, Brazil*

b *Departamento de Ciências Agronômicas, Instituto Nacional de Pesquisas da Amazônia - INPA, Manaus, AM, 69011-970, Brazil*

c *Divisão de Metrologia de Materiais - DIMAT, Instituto Nacional de Metrologia, Normalização e Qualidade Industrial -INMETRO, Xerém, Duque de Caxias, RJ, 25250-020, Brazil*

Raman spectroscopy in carbon materials

Raman spectroscopy is a nondestructive technique widely used to characterize carbon in materials science, including nanotubes,[18–20] polyynes,[21] graphite,[22–24] graphene,[25–28] nanographite,[23] polycyclic aromatic hydrocarbons (PAHs),[29,30] amorphous carbons,[22,31] among others. This work examines the Raman spectra of TPI-carbons from three distinct TPI sites, presenting a comparison between the TPIs and two different materials: (1) diamond-like carbon (DLC) films heat treated at different temperatures, showing different degrees of structural organization; (2) charcoal produced in laboratory from four different plant sources. The first are well-known structures that will be used here as reference material for the attempt of structural characterization of the TPIs. The second is the prototype for the generation of '*Terra Preta Nova*' (New Dark Earth), an attempt to reproduce the TPIs artificially. Studies in this direction may help to propose guidelines for the attempts to reproduce the high productivity of Amazonian anthropogenic soils and thus to develop sustainable agricultural practices in the humid tropics.[15,32]

The Raman spectra of black carbon materials (TPI-carbons, charcoal, and others) performed with visible light excitation show first-order peaks between 1000 and 1800 cm^{-1}, related to the spectra of disordered graphitic (or benzenoid aromatic) structures.[16] In materials with such graphitic structure, the first-order Raman spectrum is dominated by the G band ($\approx$ 1584 cm^{-1}) and the D band ($\approx$ 1355 cm^{-1} for an excitation laser energy $E_l = 2.41$ eV).[22] The G band is a first-order Raman-allowed peak attributed to the in plane tangential stretching mode of sp^2 C–C bonds.[22] The breathing-like motion of the aromatic structures gives rise to the D band peak.[22] This mode is forbidden in the first-order spectrum of crystalline graphitic structures, but it is activated by the presence of structural disorder or finite size effects in nanographites or PAHs.[22] The different relations observed between the intensities, wavenumbers and line widths of the G and D bands have been used to measure the degree of crystallinity or amorphization of graphitic materials and crystallite size in sp^2 nanographitic structures,[22,23,27,31] as will be discussed in this article.

Experimental details

Samples

Table 1 lists the samples used in this work and their respective origin. For the TPIs, the locations are near Manaus, the capital of the Amazonas state (AM) in Brazil. Field observations on TPIs, from a soil science point of view, include physical and chemical aspects that are good indicators for soil fertility. A well-balanced proportion of particle sizes provides better water holding capacity and adequate root development in physical aspect. In this perspective, TPI_{CL} exhibits the best texture (sandy clay loam) and water retention, followed by TPI_{SB} (sandy loam). The texture is medium to sandy in TPI_{BB}, providing the lowest water retention capacity in dry season (see Table 1 for the TPI nomenclature).

From the chemistry aspect, it is known that pH between 5.7 and 6.5, acting with a good proportion of macronutrients (N, P, K, Ca, Mg, and S) and micronutrients (Zn, Mn, Mo, and B), are signatures of most productive soils. In this sense, all TPI samples used in this work show good chemical indicators. More specific information about chemical attributes can be found in Ref.[16].

Table 1. Sample nomenclature and their origins

Sample	Origin
TPI_{SB}	Serra Baixa (costa do Açutuba), Iranduba (AM) (Lat. 3° 30′ S, Long. 60° 20′ W)
TPI_{BB}	Balbina, Presidente Figueiredo (AM) (Lat. 1° 54′ S, Long. 59° 28′ W)
TPI_{CL}	Costa do Laranjal, Manacapuru (AM) (Lat. 3° 18′ S, Long. 60° 33′ W)
Charcoal 1	Ingá (*Ingá edulis* Mart.)
Charcoal 2	Bamboo (*Dendrocalamus strictus*)
Charcoal 3	Lacre (*Vismia guianenses* Aubl. Pers)
Charcoal 4	Embaúba (*Cecropia hololeuca* Miq.)
DLC 1	Nanographite (DLC HTT at 1200 °C)
DLC 2	Nanographite (DLC HTT at 1400 °C)
DLC 3	Nanographite (DLC HTT at 1600 °C)
DLC 4	Nanographite (DLC HTT at 1800 °C)
DLC 5	Nanographite (DLC HTT at 2000 °C)
DLC 6	Nanographite (DLC HTT at 2200 °C)
DLC 7	Nanographite (DLC HTT at 2400 °C)

Different conditions of charring generate differences among the structural organization of different TPI-carbon particles in the same TPI site. In order to characterize the general behavior of a soil sample, the Raman spectra of different TPI-carbons selected randomly were obtained for each TPI site, with 126 spectra from the three TPI sites (66 from TPI_{BB}, 30 from TPI_{SB} and 30 from TPI_{CL}). The larger number of spectra for the TPI_{BB} is due to a mapping analysis that was performed for this sample and will be discussed later in this article.

The TPI results will be compared with results from charcoal and DLCs. The charcoal samples were produced in the Charcoal Laboratory at *Instituto Nacional de Pesquisa da Amazônia* from different plant species (see Table 1) typical of Amazon region (more details in Ref.[16]). The TPIs and the charcoal samples were individually dissolved in deionized water, and a small amount was dripped on an individual cover slip. The experiment was performed for each sample after dried in ambient conditions.

The DLC films were used as reference material to perform structural classification of carbon forms found in the TPI soil samples. The DLC samples were produced by a pulsed laser deposition method, and the target used was highly oriented pyrolytic graphite (HOPG) in vacuum conditions (5×10^{-6} Torr).[23] An electrical furnace setup was used to anneal the samples at heat treatment temperatures (HTTs) of 1200°, 1400°, 1800°, 2000°, 2200°, and 2400 °C. While the heat treatment was happening, the samples were kept inside a closed graphite tube under an argon atmosphere (inert gas with 99.999% purity) flowing at 1 l/min.

Instrumental details

For statistical analysis and spectral mapping, the Raman scattering measurements were performed with an Andor™ Tecnology-sharmrock sr–303i spectrometer coupled with a charge coupled device detector, in the backscattering configuration using 60× oil immersion and air objective lenses. Excitation light was provided by a 633 nm (1.96 eV) He–Ne laser. For the measurements performed on soil samples, the oil immersion objective lens was used, and the laser power was (140 ± 10) μW at the sample. The measurements on DLC and charcoal samples were performed with

Journal of RAMAN SPECTROSCOPY

the air objective lens and laser power of (265 ± 10) μW at the sample. The spectral resolution is 2 cm^{-1}.

Micro-Raman scattering measurements were performed as a function of excitation laser light with a Renishaw Invia Reflex spectrometer in single mode configuration with different gratings according to excitation laser wavelength. The spectrometer resolution is better than 4 cm^{-1}, and the peak position uncertainty is around 1 cm^{-1}. We apply the backscattering configuration, using a 20× objective. Relatively low power (20 μW at the microscope objective) was used to avoid heating-induced sample damage or graphitization. The following laser lines were used: 647 nm, 514 nm, 488 nm, and 457 nm from an (Coherent Innova 70C Spectrum) Ar^+/Kr^+ laser, 442 nm and 325 nm from a (Kimmon) HeCd laser.

Spectral fitting procedure

The Raman spectrum from the TPI-carbon samples in dispersive Raman usually displays background signals, which are stronger in the visible and weaker in the ultraviolet (UV) excitation range. For statistical analysis, it is important to clearly define a protocol for the exclusion of baseline, necessary to access the Raman spectroscopic information. The procedure used to all spectra was the exclusion of a linear baseline between 800 cm^{-1} and 1900 cm^{-1}. The same procedure, for all spectra, guarantees the detection of differences related to structural physical properties among the studied material. In Fig. 1 (a), the extracted baseline is exemplified.

The D and G Raman band shapes can be analyzed by a set of variables that indicates the degree of sp^2 e sp^3 hybridization and the crystallinity of graphitic materials.[31–36] The fitting procedure was performed using two Lorentzian peaks [see Figure 1 (b)], defining the parameters that are used in our study, namely the integrated area of the D and G peaks (A_D and A_G, respectively), the G band wavenumber (ω_G), and the G band full-width at half maximum (Γ_G). The D band wavenumber and full-width at half maximum were observed in the range 1345 $cm^{-1} < \omega_D < 1360$ cm^{-1} and 210 $cm^{-1} < \Gamma_D < 270$ cm^{-1}, independent on the TPI site, and we do not discuss these results in depth. Small peaks around 1020 cm^{-1}, 1180 cm^{-1}, 1450 cm^{-1}, and 1790 cm^{-1} were observed in the Raman spectra of the TPI samples in the visible range, even when the black carbon signal is not present. Therefore, these peaks are not related to the TPI-carbon structures, being disregarded in our analysis. Important to state that these peaks are always weak as compared to the TPI carbon signal in all the spectra we analyzed, as shown in Fig. 1. Consequently, they do not influence the D and G fitting parameters.

The fitting of DLC spectra were similar to the procedure described above, but using an additional disorder-induced peak know as D′ band (≈ 1610 cm^{-1}), which clearly appears for HTTs at 1800 °C and above (see Figure 2). For HTTs above 1800 °C, the D and D′ bands intensities decrease, leading to a typical spectrum of HOPG for HTTs above 2400 °C. The evolution of the Raman spectra of carbons along an amorphization trajectory, from perfect graphite or graphene to fully disordered tetrahedral amorphous carbon have been organized and classified in three stages.[31] In the study of TPI-carbons, stages 1 and 2[27,28,31] are the most relevant and are summarized below.

Within stage 1, the Raman spectral evolution from perfectly crystalline graphite to nanocrystalline graphite shows the appearance of the D and D′ peaks followed by an increase in the intensity ratio (A_D/A_G) between the D and G bands; all peaks broaden and the G

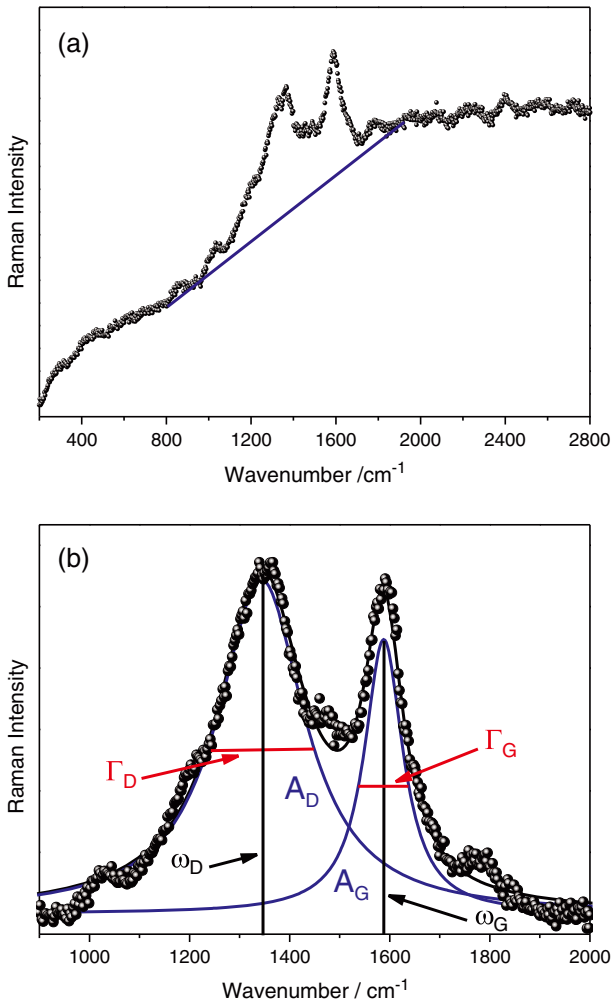

Figure 1. (a): Procedure performed for baseline exclusion. A linear baseline between 800 cm^{-1} and 1900 cm^{-1} was excluded in all spectra of TPI samples. (b): example of the fitting procedure using two Lorentzian peaks. The relevant parameters for our studies are: integrated area of D (A_D) and G (A_G) peaks, G peak wavenumber (ω_G) and full-width at half maximum (Γ_G). Spectrum obtained with the 633 nm laser.

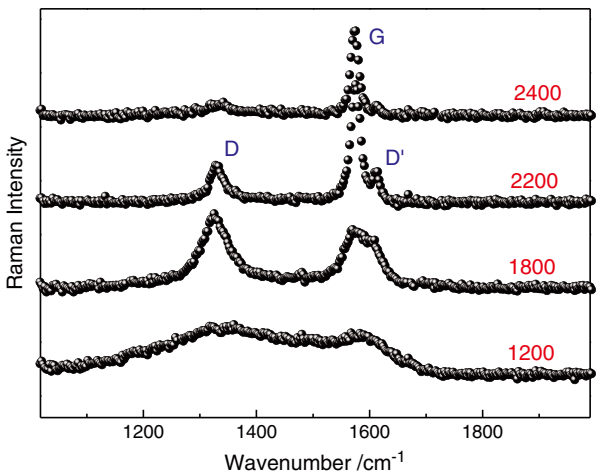

Figure 2. Spectra of DLC films obtained at different heat treatment temperatures, as indicated in Celsius degree units close to each respective spectrum. The D, G, and D′ peaks are also indicated. Spectra obtained with the 633 nm laser.

band overlaps with the D′ generating a wide band that upshifts in wavenumber to ~ 1600 cm^{-1}. The G band wavenumber is mostly independent on the excitation laser energy.

Within stage 2, the Raman spectral evolution from nanocrystalline graphite to low sp^3 amorphous evolves as follows: the G peak position decreases from $\omega_G \sim 1600\,cm^{-1}$ towards $\omega_G \sim 1510\,cm^{-1}$; the A_D/A_G decreases towards 0; ω_G becomes dispersive with the excitation laser energy, the dispersion increasing with disorder. For excitation in the UV the G band is observed at $\omega_G \sim 1690\,cm^{-1}$ when higher contents of sp^3 carbons are present.

Results and discussion

Structural disorder and the sp^2 *versus* sp^3 hybridization

Figure 3 shows the analysis of ω_G as a function of Γ_G for DLC films (filled bullets connected by dashed lines) and the TPI-carbons (open symbols). The as-grown DLC starts as hydrogenated tetrahedral amorphous carbon (ta-C:H) with relatively low ω_G, while the other filled bullets data have been heat treated at different temperatures as indicated in the figure. The ta-C:H without heat treatment showing the lowest G band wavenumber and the largest Γ_G is characteristic of amorphous carbon majorly composed by sp^3 hybridization (see filled bullet in Fig. 3 labeled with 'as grown'). For HTTs above 600 °C, the processes of hydrogen expulsion and structural changes take place.[33] At higher treatment temperatures, hydrogen is progressively released, and there is an increase of the sp^2 to sp^3 ratio accompanied by an increase in the wavenumber of the G band (see filled bullets connected by dashed lines in Fig. 3). The sp^3 carbon phase is completely extinguished for HTTs above 1600 °C, giving place to sp^2 nanographite crystals.[34] The DLC in-plane crystallite size L_a increases by increasing heat-treatment temperatures above

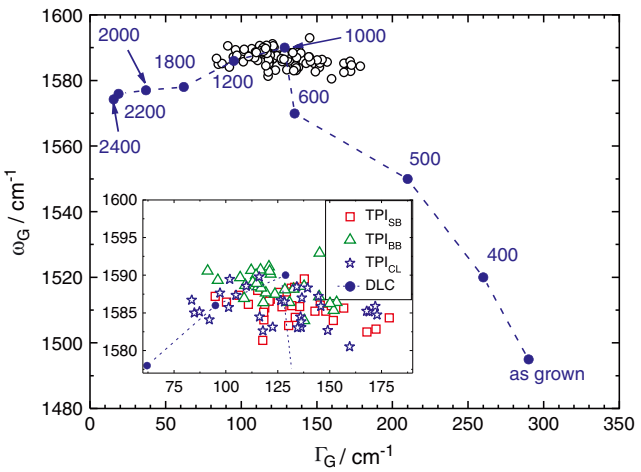

Figure 3. G band frequency (ω_G) *versus* full width at half maximum (Γ_G) for the G band of DLCs and TPI-carbons. Filled bullets connected by dashed lines stand for DLC (data for DLC as grown, 400°, 500°, 600°, and 1000° are found in Ref.[33]), and open bullets stand for an ensemble of 90 Raman spectra of TPI-carbon samples (30 from each site). The notations near the DLC data give the HTT (°C) for the respective sample. The inset shows a magnification where it is possible to distinguish the three TPI samples. The open bullets in the main panel represent all the TPI samples together. The G band was fit with one Lorentzian for all TPI-carbons and for the DLCs heat treated at 1800° and below. For DLCs heat treated at 2000° and above, we used two Lorentzians (see related discussion at the supporting information).

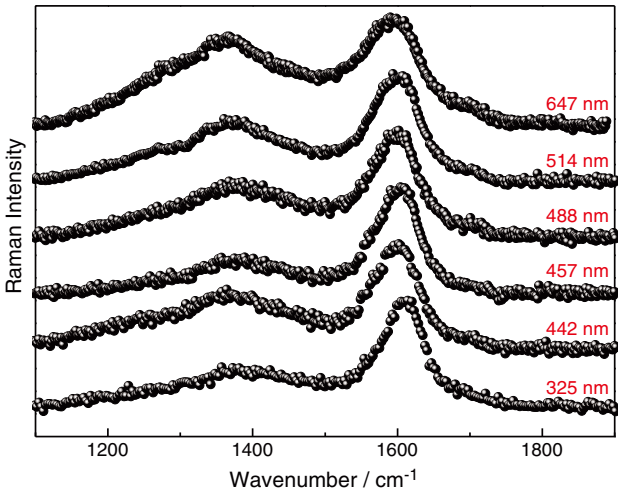

Figure 4. Raman spectra of TPI-carbon found in TPI_{CL} sample obtained with different excitation laser lines. The excitaiton laser wavelengths are indicated in the figure.

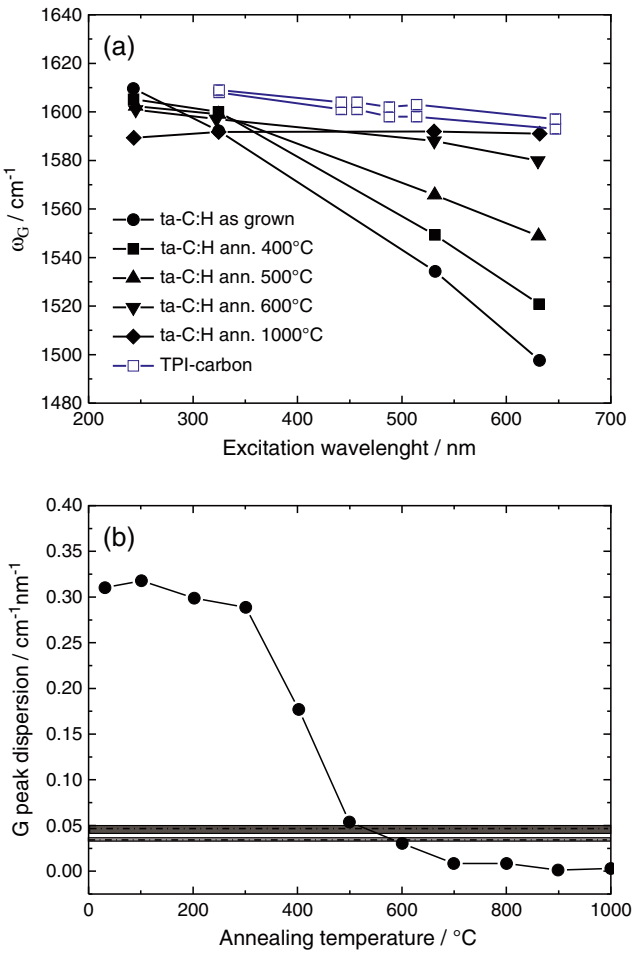

Figure 5. (a): G band peak dispersion *versus* excitation wavelength for ta-C:H samples annealed at different temperatures (filled symbols, data from Ref.[33]) and for two TPI-carbons found in the TPI_{CL} sample (open squares). (b): G peak dispersion for ta-C:H annealed at different temperatures (symbols, data from Ref.[33]). The dot-dashed lines indicate the dispersion values found for the two TPI-carbons, while the gray areas correspond to their respective error bars.

Journal of RAMAN SPECTROSCOPY

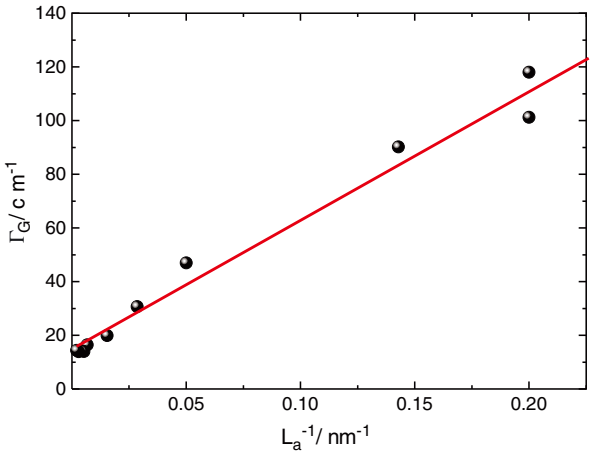

Figure 6. Linear relation between Γ_G and $1/L_a$ (L_a is the average in-plane crystallite size) for the DLC spectra obtained using the 514 nm laser. The filled bullets are experimental data, and the solid line is the linear fit giving rise to Eqn (1).

1600 °C, as determined by X-ray diffraction and scanning tunneling microscopy.[23] Comparing the data from the TPIs with the data of DLC under thermal treatment, the TPI-carbon Raman signal excited with the 633 nm laser comes majorly from sp^2 carbon-like structures.

Within the experiments discussed above, it is not possible to rule out the presence of some sp^3 hybridized material in the TPI samples, because the visible light excites mostly the sp^2 π electron bands.[31] The optical signal related to the σ electronic states, common to both sp^2 and sp^3 structures, become detectable with UV Raman spectroscopy.[37] Figure 4 corresponds to the Raman spectra of a TPI-carbon in the TPI_{CL} sample acquired with different excitation wavelengths. The D and G bands are clearly observed in all wavelengths. The position of D band changes from 1385 cm^{-1} at 325 nm light excitation to 1364 cm^{-1} at 647 nm light excitation, as expected for sp^2 carbons.[18–20,26,33] On the other hand, the G band is known to be dispersive only in amorphous carbon materials, and this dispersion is proportional to the level of sp^3 hybridization.[33] Figure 5(a) shows the behavior of the G band wavenumbers with different wavelengths of excitation for ta-C: H heated at different temperatures (data form Ferrari and Robertson, Ref.[33]) and for two different TPI-carbons found in the TPI_{CL}. The minor dispersion of the G band for the TPI-carbons confirms their structure is characterized predominantly by sp^2 carbons.

Figure 5 (b) is a restatement of the conclusions presented above. The slope obtained from the linear fit of two TPI-carbon data is compared with the dispersion of several heat treated ta-C:H samples. The dot-dashed line indicates the dispersion value of the TPI-carbon data. The values found for TPI-carbon dispersions are already set among the ta-C:H with high treatment temperatures and low dispersion values, indicating a majorly sp^2 carbonaceous material present in the TPIs.

Structural disorder and the crystallite size (L_a)

The results in the previous section parameterize the TPI-carbons within the limit range between the graphite amorphization stages 1 and 2, where the key parameter is the in-plane size of the sp^2 structures. The Raman spectra of DLCs have been well characterized with respect to the average crystallite size in the samples (L_a), which depends also on the HTT.[22,23,31,32] Figure 6 shows the linear dependence between the G band full width at half maximum (Γ_G) and the inverse of the average crystallite size (L_a^{-1}) for DLCs, as measured by X-ray diffraction[23] for the DLCs analyzed in this work. The data can be fit with

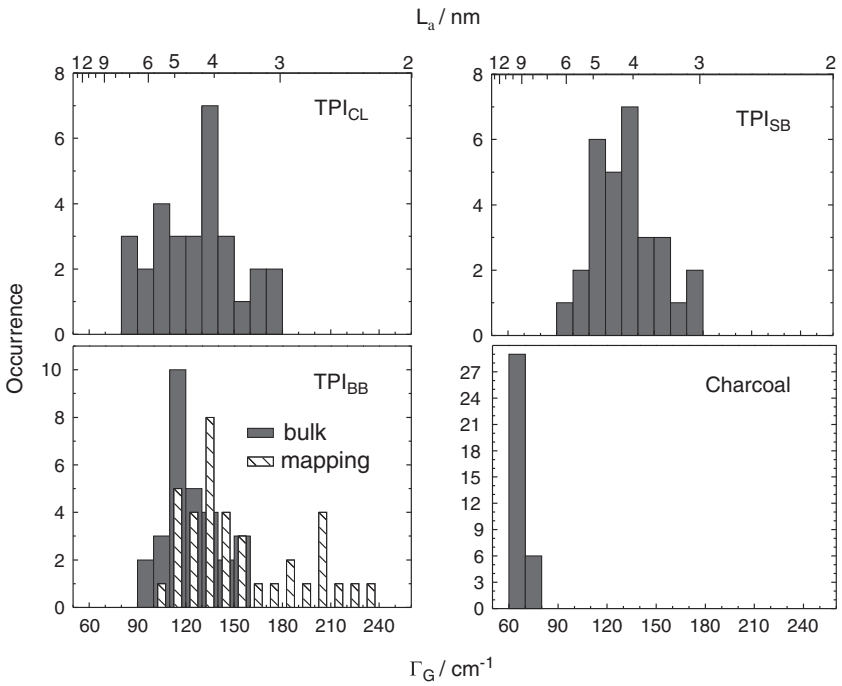

Figure 7. Occurrence *versus* G band full width at half maximum (Γ_G) for 126 TPI-carbons (66 from TPI_{BB}, 30 from TPI_{SB} and 30 from TPI_{CL}) and 35 charcoal samples, all measured with the 633 nm laser. There is a larger number of data for the TPI_{BB} because data from single grain mapping procedures (hashed bars) were added here. This procedure pushes the distribution of measured Γ_G to higher values, as discussed in the text. The top axis gives the average crystallite size (L_a) according to Eqn (1).

$$L_a(nm) = 496/[\Gamma_G - 15], \quad (1)$$

which is in good agreement with Ref.[38] within the L_a range measured here.

Figure 7 corresponds to the occurrence of measured Γ_G for the 126 different TPI spectra. Each count corresponds to a spectrum taken from a distinct point of the sample where black carbon structures were identified. Generally speaking, the three TPI-carbons exhibit similar Γ_G distribution, while the charcoal samples exhibit a Γ_G distribution clearly distinct from the TPI-carbons.

To gain insight about the structural aspect behind the results of Figure 7, Eqn (1), which applies to a broad range of carbon nanostructures from nanographite to amorphous carbon,[23,34] is used as an attempt to access the average crystallite size (L_a) in the soil samples and the charcoal produced in laboratory. According to Eqn. (1), the typical L_a sizes present in TPI-carbons were found between 2 and 8 nm (see top X-axis in Fig.7), thus placed on the threshold between the Raman characteristics exhibited by amorphous carbon (stage 2) and graphitic nanostructures (stage 1).[27,28,31] In comparison, the charcoal sample produced in laboratory presents L_a larger than soil samples, ranging from 7 to 11 nm, lying on nanocrystalline graphitic behavior,[27,28,31] where the sp^2 hybridization typical of a more graphitized arrangement is predominant.

From Fig. 7, the TPI-carbon samples are clearly different from that charcoal produced in laboratory, the latter showing a higher degree of crystallinity (larger in-plane L_a nanocrystallite sizes). This can be related to the degradation (oxidation) process of the black carbons present in TPI soils over the years.[16] This is important for soil fertility improvement because (1) the oxidation of aromatic rings gives rise to broken links enhancing the cation exchange capacity of soils by the chemical bond with nutrients;[2] (2) the small crystallite sizes allows Ca, O and P to diffuse in the carbonaceous structure;[16] and (3) the aromatic structure is responsible to the prolonged stability against microbial degradation and leaching.

Mapping the structural disorder from the core to the surface of a single TPI-carbon particle

To explore the considerable spread in Γ_G (or L_a) for the measured TPI-carbons, we performed more in depth analyses on isolated TPI-carbon grains, and the TPI-carbon grains were shown to exhibit a different structure in the core and at the surface.[16,39] The mapping of the Raman spectra from core to grain surface is capable to reveal changes in the crystallite structure. A TPI-carbon grain was selected and sectioned in a way that the interface was turned to a cover slip and a G-band spectral imaging was acquired. It was then possible to measure specific points from the interior (core) to the exterior (surface) region of the TPI-carbon grain.

Figure 8 (a) shows the Raman spectra taken from the core to the surface of a TPI-carbon grain. Comparing the spectra from the bottom to the top, there is an evolution of overlap between the D and G peaks, related to an increase in Γ_G. For example, Γ_G (bottom spectra) = 108 cm^{-1} and Γ_G (top spectra) = 207 cm^{-1}. Using Eqn (1), the average crystallite size in the center of the carbon structure is L_a (core) = 5.3 nm, while at the surface L_a (surface) = 2.6 nm. Figure 8 (b) corresponds to the relation between Γ_G (and L_a) and the distance from the core to the surface for three mapping procedures similar to that shown in Fig. 8 (a). The behavior is similar along all the core–surface interfaces, i.e. a gradual increase in Γ_G (decrease in L_a) is observed when the laser focus is moved from the core to the surface. These results indicate that the disordering (oxidation) process was more effective at the surface, in agreement with previously published analysis.[16,39] The reactivity is provided by smaller crystallite sizes in the periphery, whereas the stability of this material is related to larger crystallite sizes dominant in the core. Notice that the Γ_G values show in Fig. 7 are dominated by values consistent with those of the core spectra.

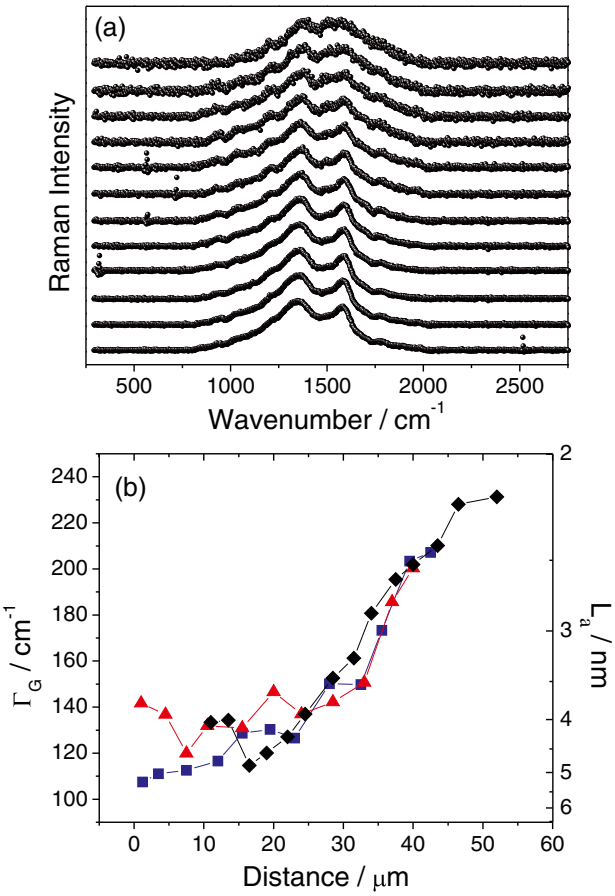

Figure 8. (a): Raman spectra at different locations of an isolated TPI-carbon grain, moving from core (bottom) to the surface (top). (b): Γ_G (or L_a) *versus* distance from the core to the surface for three different mapping procedures (different symbols). Measurements performed on a TPI-carbon grain found in the TPI_{BB} sample. Data obtained with the 633 nm laser.

Finally, the same analysis discussed here were performed using the 325 nm UV laser light. In the UV, the observed Γ_G values are generally smaller than those found in the visible range, by about 35%. Since Eqn (1) was parameterized in the visible, the quantitative L_a analysis presented here is restricted for this range. However, all the comparative L_a evolution analysis (TPI-carbons *vs* charcoal, core *vs* surface) found in the UV is qualitatively consistent with those found in the visible range excitation. It is important to state also that the core vs surface analysis was not performed in the charcoals, since the as-produced samples are homogeneous materials and any grain structure is an effect of the powdering procedure.

Conclusions

Raman spectroscopy was used to characterize the structure of the carbon material found in the *Terras Pretas de Índio* (TPI-carbon)

from the Amazon Forest. The analysis is based on the comparison of the TPI-carbon results with those from laboratory produced reference materials, such as charcoal and heat treated DLCs.

The Raman spectra of the TPI-carbons indicate that their sp^2 to sp^3 contents and crystallite sizes L_a are typical of structures within the limit region between nanographite and amorphous carbons, labeled stages 1 and 2 of carbon amorphization in the literature.[27,28,31] Although this result relies on the use of Eqn (1), which is not independently determined for the TPI-carbons, the statement is robust and provides two important conclusions. First, TPI soils exhibit unusually high stability (over millennia) and fertility over long agricultural usage time (tens of years); second, the interface between stages 1 and 2 is likely to provide the best balance between stability and reactivity of the carbon nanostructures.[16] The mapping of the crystallite size from the core to the surface of a single TPI-carbon grain shows that the structural graphitic disorder at the surface is more prominent than in the core, thus providing a suitable structure for the TPI-carbons, where the grain surface offers a more reactive environment for adsorption and release of nutrients, while the core provides a very stable sink for soil stability. Furthermore, comparison of the TPI results with those from charcoal produced in laboratory showed that the charcoal samples present higher crystallinity, i.e. a more inert material, probably less appropriated for improving soil fertility.

We have thus shown that the Raman spectroscopy can be used as an important tool for analyzing the structure of black carbon present in soils, deeply related to fertility and resilience. This technique may be used as a guide in attempts to reproduce the TPI-carbons for the generation of artificial '*Terra Preta Nova*' (New Dark Earth), thus generating new opportunities for sustainable agriculture.

Acknowledgements

The authors acknowledge A. C. Ferrari for critical reading of the manuscript. This work was supported by FAPEMIG (PPM and Pronex BioNC), CNPq (Universal grant), FINEP and FAPERJ.

Supporting information

Supporting Information may be found in the online version of this article.

References

[1] D. C. Kern, G. D'Aquino, T. E. Rodrigues, F. J. L. Frazão, W. Sombroek, T. P. Myers, E. G. Neves, in Amazonian Dark Earths: Origin, Properties, Management, (Eds: J. Lehmann, D. C. Kern, B. Glaser, W. I. Woods) Kluwer Academic Publishers, Dordrecht, **2003**, pp. 51–75.
[2] B. Glaser, *Phyl. Trans. R. Soc.* **2007**, *362*, 187.
[3] N. J. H. Smith, *Ann. Assoc. Am. Geogr.* **1980**, *70*, 553.
[4] B. Glaser, J. Lehmann, W. Zech, *Biol. Fertil. Soils* **2002**, *35*, 219.
[5] B. Liang, J. Lehmann, D. Solomon, J. Kinyangi, J. Grossman, B. O'Neill, J. O. Skjemstad, J. Thies, F. J. Luizão, J. Petersen, E. G. Neves, *Soil Sci. Soc. Am. J.* **2006**, *70*, 1719.
[6] C. H. Cheng, J. Lehmann, *Chemosphere* **2009**, *75*, 1021.
[7] L. Haumaier, W. Zech, *Org. Geochem.* **1995**, *23*, 191.
[8] E. H. Novotny, M. H. B. Hayes, B. E. Madari, T. J. Bonagamba, E. R. de Azevedo, A. A. de Souza, G. Song, C. M. Nogueira, A. S. Mangrich, *J. Bra. Chem. Soc.* **2009**, *20*, 1003.
[9] B. Glaser, L. Haumaier, G. Guggenberger, W. Zech, *Naturwissenschaften*, **2001**, *88*, 37.
[10] J. Lehmann, M. Rondon, in Biological Approaches to Sustainable Soil Systems, (Eds: N. Uphoff, A. S. Ball, E. Fernandes, H. Herren, O. Husson, M. Laing, C. Palm, J. Pretty, P. Sanchez, N. Sanginga, J. Thies), CRC Press/Taylor & Francis Group, Florida, **2006**, pp. 517–526.
[11] C. Steiner, W. G. Teixeira, J. Lehmann, T. Nehls, J. L. V. de Macêdo, W. E. H. Blum, W. Zech, *Plant Soil* **2007**, *291*, 275.
[12] J. Lehmann, *Nature* **2007**, *447*, 143.
[13] E. G. Neves, J. B. Petersen, R. N. Bartone, M. J. Heckenberger, in Amazonian Dark Earths: Explorations in Space and Time, (Eds: B. Glasser, W. I. Woods), Springer, Berlin, **2004**, pp. 125.
[14] W. Sombroek, M. L. Ruivo, P. M. Fernside, B. Glaser, J. Lehmann, in Amazonian Dark Earths: Origin, Properties, Management, (Eds: J. Lehmann, D. C. Kern, B. Glaser, W. I. Woods) Kluwer Academic Publishers, Dordrecht, **2003**, pp. 125–140.
[15] C. C. Mann, *Science* **2002**, *297*, 920.
[16] A. Jorio, J. Ribeiro-Soares, L. G. Cançado, N. P. S. Falcão, H. F. Dos Santos, D. L. Baptista, E. H. Martins Ferreira, B. S. Archanjo, C. A. Achete, *Soil Till. Res.* **2012**, *122*, 61.
[17] B. Glaser, E. Balashov, L. Haumaier, G. Guggenberger, W. Zech, *Org. Geochem.* **2000**, *31*, 669.
[18] A. Jorio, M. A. Pimenta, A. G. Souza Filho, R. Saito, G. Dresselhaus, M. S. Dresselhaus, *New J. Phys.* **2003**, *5*, 139.1.
[19] R. Saito, M. Hofmann, G. Dresselhaus, A. Jorio, M. S. Dresselhaus, *Adv. Phys.* **2009**, *60*, 413.
[20] S. Reich, C. Thomsen, J. Maultzsch, Carbon Nanotubes: Basic Concepts and Physical Properties, Wiley-VCH, Weinheim, **2004**.
[21] A. K. Ott, G. A. Rochtsteiner, C. Felix, O. Hampe, M. F. Farrold, R. P. Van Duyne, *J. Chem. Phys.* **1998**, *109*(22), 9652.
[22] F. Tuinstra, J. L. Koenig, *J. Chem. Phys.* **1970**, *53*, 1126.
[23] L. G. Cançado, K. Takai, T. Enoki, M. Endo, Y. A. Kim, H. Mizusaki, A. Jorio, L. N. Coelho, R. Magalhães-Paniago, M. A. Pimenta, *Appl. Phys. Lett.* **2006**, *88*, 163106.
[24] M. S. Dresselhaus, G. Dresselhaus, K. Sugiharam, I. L. Spain, H. A. Goldberg, M. Cardona. Graphite Fibers and Filaments. Springer-Verlag Ser. in Mater. Sci. vol 5, Berlin, **1988**.
[25] A. C. Ferrari, J. C. Meyer, V. Scardaci, C. Casiraghi, M. Lazzeri, F. Mauri, S. Piscanec, D. Jiang, K. S. Novoselov, S. Roth, A. K. Geim, *Phys. Rev. Lett.* **2006**, *97*, 187401.
[26] A. Jorio, R. Saito, G. Dresselhaus, M. S. Dresselhaus, Raman Spectroscopy in Graphene Related Systems, Wiley-VCH Verlag GmbH & Co KGaA, Weinheim, **2011**.
[27] M. M. Lucchese, F. Stavale, E. H. Martins Ferreira, M. V. O. Moutinho, R. B. Capaz, C. A. Achete, A. Jorio, *Carbon* **2010**, *48*, 1592.
[28] E. H. Martins Ferreira, M. V. O. Moutinho, F. Stavale, M. M. Lucchese, R. B. Capaz, C. A. Achete, A. Jorio, *Phys. Rev. B* **2010**, *82*,125429.
[29] C. Castiglioni, C. Mapelli, F. Negri, G. Zerbi, *J. Chem. Phys.* **2001**, *114*(2), 963.
[30] A. I. Alajtal, H. G. M. Edwards, M. A. Elbagerma, I. J. Scowen, *Spectroc. Acta Pt. A* **2010**, *76*, 1.
[31] A. C. Ferrari, J. Robertson, *Phys. Rev. B* **2000**, *61*, 14095.
[32] E. Marris, *Nature* **2006**, *442*, 626.
[33] A. C. Ferrari, J. Robertson, *Phys. Rev. B* **2001**, *64*, 075414.
[34] K. Takai, M. Oga, H. Sato, T. Enoki, Y. Ohki, A. Taomoto, K. Suenaga, S. Iijima, *Phys. Rev. B* **2003**, *67*, 214202.
[35] N. Wada, P. J. Gaczi, A. Solin, *J. Non-Cryst. Solids* **1980**, *35&36*, 543.
[36] S. R. Sails, D. J. Gardiner, M. Bowden, J. Savage, D. Rodway, *Diamond Relat. Mater.* **1996**, *5*, 589.
[37] J. Robertson, *Mat. Sci. Eng. R* **2002**, *37*, 129.
[38] L. G. Cançado, A. Jorio, M. A. Pimenta, *Phys. Rev. B* **2007**, *76*, 064304.
[39] J. Lehmann, B. Liang, D. Solomon, M. Lerotic, F. Luizão, J. Kinyangi, T. Schäfer, S. Wirick, C. Jacobsen, *Global Biogeochemi. Cycles* **2005**, *19*, GB1013.